Master's Thesis in Mathematics: A multi-class framework for a pedestrian cell transmission model accounting for population heterogeneity

Guy Alexander Cooper
Department of Mathematics, School of Basic Sciences, École Polytechnique Fédérale de Lausanne.

June 18, 2014

Supervisors:

Flurin Hänseler Marija Nikolić Michel Bierlaire
Transport and Mobility Laboratory, School of Architecture, Civil and Environmental Engineering,
École Polytechnique Fédérale de Lausanne.

Abstract

This work is an extension of PedCTM, an aggregate and transient cell transmission model for multidirectional pedestrian flows in which pedestrian characteristics are assumed to be homogeneous across the population considered. Critically, one fundamental diagram relating pedestrian speed and flow to local pedestrian density is employed across the entire population. This work extends the model to population heterogeneity with a multi-class approach wherein each sub-population is assigned its own characteristic fundamental diagram. The model presented requires the implementation of an update cycle to minimize numerical dispersion of pedestrians across all classes. In addition, multi-class dynamics introduces an element of competition in determining the flow constraints of the various classes. A priority scheme is implemented that allows for static, dynamic and stochastic determination of flow priorities throughout the network over the course of simulation. An attempt was made to base the class-specific fundamental diagrams off of inference from a dataset related to the PedFlux collaboration. Ultimately, however, the implementation made use of the Kladek formula for the speed-density relation. Preliminary simulations and results are presented to serve as a proof of concept.

Contents

1 Introduction

The seminal Cell Transmission Model (CTM) for simulating vehicular traffic flow is developed by Daganzo (1994) for traffic on a highway with a single entrance and exit. This model simulates the growth, propagation and dissipation of queues and accounts for vehicular shockwaves and stop-and-go traffic. Daganzo shows that the difference equation that underlies his model is a discrete analog of the differential equation used in the LWR kinematic wave model (Lighthill and Whitmann, 1855, Richards, 1956.) The LWR model simulates unidirectional vehicular traffic along a highway and can be seen as a specification of the more general continuum model for pedestrian flows in two-dimensions developed by Hughes (2002). Hughes' continuum model, in turn, forms a significant theoretical underpinning to many current pedestrian flow models. In a subsequent work, Daganzo (1995) extends his CTM to more complex network topologies that include merging and diverging branches. An earlier prototype of the Daganzo CTM is a cell based pedestrian walking model for circular flows around holy sites during pilgrimages to Mecca (Al-Ghadi and Mahmasani, 1991.) Asano (2007) extends the Daganzo CTM to account for general multidirectional pedestrian flows. This model requires *a priori* knowledge of the exact sequence of cells through which pedestrians traverse the network and uses basic pedestrian cross-flows as a test case. Critically, this work uses the same trapezoidal fundamental diagram as employed by Daganzo in the original model. This choice is justified as Seyfried (2005) shows that the velocity-density relation that underlies these models is negligibly affected by the extension from unidirectional to multidirectional flow. Guo (2011) develops an alternative pedestrian CTM for evacuation processes that does not rely on the density-flow relation. Instead, flow of pedestrians between cells depends on a system of cell potentials, cell capacity constraints and exogenously defined openings between cells.

The model developed in this work is an extension of PedCTM (Hänseler et al., 2013), a quasi-isotropic model for transient and multidirectional pedestrian flows in public walking areas that is based primarily on Daganzo's original CTM. PedCTM also makes use of the framework for multidirectional flow developed by Asano and uses the en-route path choice mechanism developed by Guo. As such, PedCTM does not need knowledge of the exact sequence of cells through which pedestrians traverse the network as was the case for the multidirectional Asano model. Critically, however, pedestrians are treated homogeneously and the model makes use of Weidmann's (1993) empirically derived fundamental diagram for the behavior of all pedestrians.

Pedestrian heterogeneity is an important factor in pedestrian flows and congestion. For example, Weidmann (1993) estimates that pedestrian free-flow speed is normally distributed with a mean of 1.34 m/s and a standard deviation of 0.34 m/s. Nikolić (2014) addresses population heterogeneity through the characterization of pedestrian flows. Her work makes use of a Voronoi tessellation similar to that employed by Steffen and Seyfried (2010) to estimate pedestrian density. In turn, a probabilistic model for the speed-density relation is employed to capture empirically observed heterogeneity. Pedestrian tracking data acquired through the PedFlux initiative is used in the calibration and validation of the model. The same dataset and methodology will be employed in this work.

There is a dearth of work done in the field of pedestrian modeling that accounts for pedestrian heterogeneity. The field is much richer, however, if the focus is expanded to include

vehicular traffic modeling. For example, Dafermos (1972) extends a traffic assignment model to handle the case of several classes of vehicle in the same transportation network with applications in street traffic with vehicles of differing sizes. In addition, Van Wageningen-Kessels (2013) develops a multi-class traffic flow model called FastLane. A principle assumption of FastLane is that all vehicles regardless of class association move at the same velocity if the system is in congestion. This assumption, while reasonable for unidirectional vehicular traffic, does not extend to pedestrian flow in the plane where congested and uncongested classes of pedestrians might conceivably coexist.

This work comprises an extension of PedCTM that accounts for population heterogeneity through a multi-class approach. Section 2 presents the general formulation of the model, including the use of an update cycle and a priority scheme for cell-to-cell flow. Section 3 outlines an attempt to base the model's underlying class-specific fundamental diagrams off of empirically inferred results. In addition, section 3 also specifies the subsequent choices made when implementing the general model numerically. Section 4 presents a series of test cases and simulations intended primarily as a proof of concept for the model. Finally, section 5 consists of a summary of the work presented, a discussion of potential issues with the model and an outline of future areas of research.

2 Model formulation

2.1 Multi-class pedestrian framework

Assume that D is the set of pedestrian classes where each class is characterized by its own fundamental diagram. Critically, each element $d \in D$ has an associated free-flow speed, v_f^d, defined as the speed at which pedestrians will travel in the absence of congestion. In turn, let v^d be the space-mean speed of pedestrian class d, which is the average speed of the associated pedestrians per unit space. We assume that the value of the space-mean speed at a particular location is a function only of the total pedestrian density at the location considered. Thus we have that

$$v^d = v^d(k) = v^d\Big(\sum_{d\in D} k^d\Big), \tag{1}$$

where k is the density of pedestrians at the considered location and k^d is the density of only class d pedestrians. The functional form of the space-mean speed of each class is left unspecified but will critically depend on the values of the parameters v_f^d, $\forall d \in D$.

In the homogeneous model, the specific flow q (defined as the number of pedestrians passing a pre-determined threshold per unit time and space) is modeled as the product of pedestrian density and space-mean speed using results from hydrodynamic theory. In the heterogenous extension, we define a class-specific flow as

$$q^d = k^d v^d(k) = k^d v^d\Big(\sum_{d\in D} k^d\Big), \tag{2}$$

where q^d is the number of pedestrians of class d that pass through a threshold per unit time and space. Importantly, if the density of all pedestrian classes save one are set equal to

zero, then the heterogenous extension recovers the form of specific flow as specified in the homogeneous model.

2.2 Cell network structure

The spatial discretization scheme remains unchanged from that developed in the homogeneous model by Hänseler et al. [8]. Space is discretized into square cells ξ of uniform length ΔL. Each cell has an area A_ξ that may be less than ΔL^2 if physical obstacles are present. The cell network, in turn, is represented by a directed graph $G = (\mathcal{X}, \mathcal{Y})$ where $\mathcal{X}$ is the set of cells ξ and $\mathcal{Y}$ is the set of directed links connecting cells one to another. Adjacent cells are connected to each other if they share a cell edge and the set of neighbors of a cell ξ is denoted $\mathcal{N}_\xi$.

We now presume that there are a finite number of routes R along which a pedestrian can traverse the cell network. A route $\rho \in R$ is defined as a sequence of areas without loops, $\rho = (\rho_0, \rho_1, \ldots, \rho_r)$, where each of these areas, ρ_i, represents a non-empty and connected subgraph of G. In this scheme, the first and last areas ρ_0 and ρ_r are boundary "areas" that consist of exactly one cell each, can be adjacent to an arbitrary number of cells and have no capacity constraints. Critically, there can be several routes connecting the same boundary cells but each route must begin and end at a boundary cell and there cannot be a boundary cell in a position that is not the first or last area of the route.

Time is discretized into a set of T intervals where the intervals $\tau \in \{1, 2, \ldots, |T|\}$ are of uniform length Δt. The heterogenous model requires the implementation of an update cycle and, as such, the value of Δt is an important choice and represents a significant departure from the homogeneous model. This formulation is developed in the next subsection.

The aggregation of pedestrians occurs at the level of pedestrian groups indexed by $\ell \in \mathcal{L}$. Each group ℓ is defined by a shared route along the network $\rho_\ell \in R$, emanating during a shared time interval $\tau_\ell \in T$ and belonging to the same pedestrian class $d_\ell \in D$. The set of pedestrian groups is thus a subset of the cross product of the associated sets: $\mathcal{L} \subset R \times T \times D$. Pedestrian demand through the network over the time course considered can be summarized succinctly by knowledge of the number of pedestrians in each pedestrian group $\ell \in \mathcal{L}$ and denoted by X_ℓ. In this work we presume that pedestrian demand (X_ℓ, $\forall \ell \in \mathcal{L}$) is known *a priori*.

Thus, in our discretization of space we assume that pedestrian density is uniform at the levels of individual cells. The number of pedestrians in a cell ξ at a time interval τ is given by

$$M_{\xi,\tau} = \sum_{\ell \in \mathcal{L}} M^\ell_{\xi,\tau}, \tag{3}$$

where $M^\ell_{\xi,\tau}$ is the number of pedestrians belonging to group ℓ in the cell ξ at time τ. Trivially, the number of pedestrians belonging to a specific class $d \in D$ in a cell ξ at a time interval τ is calculated as

$$M^d_{\xi,\tau} = \sum_{\ell \in \mathcal{L}} M^\ell_{\xi,\tau} \mathbb{1}_{d_\ell = d} \tag{4}$$

and is equal to $k^d_{\xi,\tau}A_\xi$ with $k^d_{\xi,\tau}$ as the uniform density of pedestrian class d for cell ξ at time τ. We now turn to the choice of Δt in the heterogenous pedestrian model.

2.3 Discretization of time and the update cycle

In the homogeneous model, the time step interval size is chosen so as to guarantee that $v_f\Delta t = \Delta L$ and thus minimize numerical dispersion of pedestrians. In the heterogenous framework, we maintain this numerical approximation scheme by defining separate time interval discretizations for each pedestrian class. Thus, $\Delta t^d = \Delta L/v^d_f$ is the time interval associated to each pedestrian of class d. Having defined these class-specific time intervals we calculate the global time interval discretization as

$$\Delta t = gcd(\{\Delta t^d\}_{d\in D}). \tag{5}$$

Consequently, for each $d \in D$ we have that $\Delta t^d = \alpha^d \Delta t$ where α^d is a positive integer. Pedestrians of the same class d that enter the system during the same interval τ will only be updated every α^d time steps from the time of departure. For the purposes of model simplicity, we assume that pedestrians groups can only enter the cell network at a time interval that is a constant multiple of the group's α^d value. This assumption should not lead to unwanted effects as long as the scale of the pedestrian group travel times are much greater than the associated time interval discretization sizes. We now consider in more detail the discretization of flow in the heterogenous model.

2.4 Flow capacities and the priority scheme

Let $Q^d_{\xi\to\nu,\tau}$ be the cumulative hydrodynamic flow of pedestrian class d from cell ξ to cell ν during interval τ. This is the number of class d pedestrians that pass through the link in α^d time intervals assuming that all the pedestrians of class d in cell ξ will attempt to "flow" to ν during τ. The class-specific cumulative hydrodynamic flow is thus calculated as

$$Q^d_{\xi\to\nu,\tau} = \int_0^{\Delta t^d}\int_0^{\Delta L} q^d dt dL = m^d_{\xi\to\nu,\tau}\frac{v^d(m_{\xi\to\nu,\tau})}{v^d_f}, \tag{6}$$

where $m^d_{\xi\to\nu,\tau}$ is the unknown quantity of class d pedestrians that attempt to traverse the link during the current time step and $m_{\xi\to\nu,\tau}$ is the sum of those quantities over all pedestrian classes. In the homogeneous case, the cumulative hydrodynamic flow is cell-specific and is characterized by its maximum value $Q_{\xi,opt}$ and the value of $m_{\xi,\tau}$ at which this maximum occurs, $M_{\xi,opt}$. The domain is thus partitioned into two regimes. For values of $m_{\xi,\tau}$ less than $M_{\xi,opt}$, a small increase in pedestrian mass leads to increased cumulative hydrodynamic flow and is thus denoted as the free-flow regime. Conversely, the congested regime consists of the values of $m_{\xi,\tau}$ greater than $M_{\xi,opt}$ as an increase in pedestrian mass in this domain leads to a decrease in overall cumulative hydrodynamic flow. The outflow capacity is then defined as equal to the cumulative hydrodynamic flow, $Q^d_{\xi,\tau}$, if the actual number of pedestrians in the cell $M_{\xi,\tau}$ is in the free-flow regime and set equal to $Q_{\xi,opt}$ if it is in the congested regime.

The inflow capacity is equal to $Q_{\xi,opt}$ in the free-flow regime and otherwise is equal to the cumulative hydrodynamic flow, $Q^d_{\xi,\tau}$, in the congested regime.

This process of decomposing the domain into free-flow and congested regimes and deriving the inflow and outflow capacities is less straightforward in the heterogenous case as we now deal with class- and link-specific cumulative hydrodynamic flows, each of which is a multivariable function of $|D|$ dimensions[1]. Without loss of generality, let us consider only the cumulative hydrodynamic flow for pedestrians of class d along the link from cell ξ to ν, and derive the class- and link-specific inflow capacity $\hat{Q}^d_{\xi\to\nu,\tau}$ and outflow capacity $\tilde{Q}^d_{\xi\to\nu,\tau}$.

One possible choice for the values of $(m^{d'}_{\xi\to\nu,\tau})_{d'\in D}$ is to set them all exactly equal to their counterparts in $(M^{d'}_{\xi,\tau})_{d'\in D}$, save that of the class d we are interested in. We then partition the domain into the respective free-frow and congested regimes by the optimal cumulative hydrodynamic flow over $m^d_{\xi\to\nu,\tau}$. Ease of computations is a clear advantage of this method as a multidimensional optimization problem has been reduced to one dimension and the derivation of the inflow and outflow capacities is then identical to that of the homogeneous model. However, the behavioral implications of this choice are problematic, particularly with respect to the outflow capacity. When determining its own outflow capacity along a link, each class of pedestrians presumes that the entire local mass of pedestrians belonging to all other classes will attempt to flow through the link in the next time step. This constitutes a worst-case approximation on the part of all classes and can lead to artificial congestion in the network. Another option is to simply set all $(m^{d'}_{\xi,\tau})_{d'\in D}$, save that of class d, to zero and partitioning the domain similarly. This leads to the inverse problem, however, as each class will then presume that none of the other classes will use the considered link in the next time step. As a result, there will be no interaction or competition between the respective classes when calculating flow capacities and thus the flow of pedestrians through the network will be artificially high.

A compromise between the two proposed methods that nonetheless maintains an ease of computation is to suppose that each class flows through the link in turn, one after another, in an orderly fashion. The classes are thus sorted into a priority structure where the classes higher in the priority scheme flow before those that are lower. Thus, the inflow and outflow capacities along a link for a specific class are constrained by the flow of pedestrian classes with higher priority but not by those with lower priority. This leads to a similar reduction to one dimension as seen before, where $Q^d_{\xi\to\nu,\tau}$ is now optimized only along the axis of $m^d_{\xi\to\nu,\tau}$. All other values of $m^{d'}_{\xi\to\nu,\tau}$ such that $d'\neq d$ are held fixed according to the scheme

$$m^{d'}_{\xi\to\nu,\tau} = \begin{cases} S^{d'}_{\xi\to\nu,\tau}, & \text{if } d' > d \text{ in priority,} \\ 0, & \text{otherwise,} \end{cases} \tag{7}$$

where $S^{d'}_{\xi\to\nu,\tau}$ is the sending capacity of class d' pedestrians along the link and is specified in the subsequent subsection. We see that the class with the highest priority is unconstrained by the flow of any other class and is treated identically to the pedestrians in the homogeneous model. For each class, once the domain partition and specification of Equation (6) has been determined, the derivation of the associated inflow and outflow capacity along the link is identical to that of the homogeneous model with evaluation of the function at the number of

[1]or 2 dimensions if the second variable is taken to be the sum $m_{\xi\to\nu,\tau}$.

associated pedestrians in the cell ξ at time step τ. A significant consequence of this approach is that the class-specific outflow and inflow capacities as well as the class-specific sending capacities must be calculated in a sequential manner in the order of the priority scheme of the associated cell.

The particular form of the priority structure is arbitrary and left unspecified. Critically, the ordering of the priority scheme can be dynamic over the time course of the simulation and heterogenous across the cell network. In addition, a stochastic nature to the priority scheme can be implemented as well so that the ordering represents only the average relative class priorities. In any case, the specific class ordering of the priority structure must be determined at the start of each time step for each cell in the network.

2.5 Pedestrian flow and constraints

The sending capacity of group ℓ pedestrians from cell ξ to ν at time step τ is defined as

$$S^{\ell}_{\xi\to\nu,\tau} = \delta^{\rho_\ell,d_\ell}_{\xi\to\nu,\tau}\min(M^{\ell}_{\xi,\tau}, M^{\ell}_{\xi,\tau}\tilde{Q}^{d}_{\xi\to\nu,\tau}/M^{d}_{\xi,\tau}), \tag{8}$$

where $\delta^{\rho_\ell,d_\ell}_{\xi\to\nu,\tau}$ is the turning potential of pedestrians of class d_ℓ along route ρ_ℓ from ξ to ν at time step τ. The turning potentials must sum to one when taken over the neighbors of ξ and are determined by whatever route choice formulation is chosen. The group-specific sending capacity is critically constrained by the availability of pedestrians belonging to the group in the cell at the considered time step. In the presence of congestion, the second constraint in Equation (8) ensures that the sum of sending capacities over all groups with a shared class d will never exceed the class- and link-specific outflow capacity, $\tilde{Q}^{d}_{\xi\to\nu,\tau}$. The total sending capacity, $S^{d}_{\xi\to\nu,\tau}$, of class d pedestrians from cell ξ to ν at time step τ as seen in Equation (7) is simply the sum of the associated group-specific sending capacities over all groups with shared class d.

Having calculated the sending capacities of all groups as well as the class- and link-specific inflow capacities throughout the whole network, two more capacity constraint steps are necessary in order to determine the final flow of pedestrians in the network for the time step considered.

The first capacity constraint renormalizes each group's current sending capacity, $S^{\ell}_{\xi\to\nu,\tau}$, with respect to the link-specific class inflow capacities of the target cell ν such that

$$\mathcal{S}^{\ell}_{\xi\to\nu,\tau} = \begin{cases} S^{\ell}_{\xi\to\nu,\tau}, & \text{if } \sum_{\ell'\in\mathcal{L}} S^{\ell}_{\xi'\to\nu,\tau}\mathbb{1}_{d_{\ell'}=d_\ell} \le \hat{Q}^{d}_{\xi\to\nu,\tau}, \\ \zeta^{\ell}_{\xi\to\nu,\tau}\hat{Q}^{d}_{\xi\to\nu,\tau}, & \text{otherwise,} \end{cases} \tag{9}$$

where

$$\zeta^{\ell}_{\xi\to\nu,\tau} = \frac{S^{\ell}_{\xi\to\nu,\tau}}{\sum_{\ell'\in\mathcal{L}} S^{\ell'}_{\xi\to\nu,\tau}\mathbb{1}_{d_{\ell'}=d_\ell}}. \tag{10}$$

We thus have that the sum of the renormalized sending capacities $\mathcal{S}^{\ell}_{\xi\to\nu,\tau}$ from ξ into ν over all groups ℓ with the shared class d will never exceed the class-specific inflow capacity, $\hat{Q}^{d}_{\xi\to\nu,\tau}$, of the link. The values of $\zeta^{\ell}_{\xi\to\nu,\tau}$ ensure that sending flows from ξ into ν are apportioned according to demand if the inflow capacity along the link into the target cell is exceeded.

Having renormalized the sending capacities along all links of the network, the last capacity constraint ensures that pedestrian quantities never exceed the pedestrian capacities within the physical space available in the cells. We thus define the final flow of pedestrians belonging to group ℓ from cell ξ to ν at time step τ as

$$\mathcal{Y}^{\ell}_{\xi\to\nu,\tau} = \begin{cases} \mathcal{S}^{\ell}_{\xi\to\nu,\tau}, & \text{if } \sum_{\nu'\in\mathcal{N}_\nu}\sum_{\ell'\in\mathcal{L}}\mathcal{S}^{\ell'}_{\nu'\to\nu,\tau} \le N_\nu - M_{\nu,\tau}, \\ \psi^{\ell}_{\xi\to\nu,\tau}(N_\nu - M_{\nu,\tau}), & \text{otherwise ,} \end{cases} \tag{11}$$

where

$$\psi^{\ell}_{\xi\to\nu,\tau} = \frac{\mathcal{S}^{\ell}_{\xi\to\nu,\tau}}{\sum_{\nu'\in\mathcal{N}_\nu}\sum_{\ell'\in\mathcal{L}}\mathcal{S}^{\ell'}_{\nu'\to\nu,\tau}}. \tag{12}$$

N_ν is the cell-specific maximum number of pedestrians that can occupy cell ν at any time and $\mathcal{N}_\nu$ is the set of neighboring cells to cell ν. The values of $\psi^{\ell}_{\xi\to\nu,\tau}$ ensure that, if the sum of all incoming flows exceeds the amount of physical space available in the cell, all flows are renormalized according to a demand apportioned scheme.

We now have the final update equation for the number of pedestrians of group ℓ in cell ξ at time step $\tau+1$ as

$$M^{\ell}_{\xi,\tau+1} = M^{\ell}_{\xi,\tau} + \sum_{\nu\in\mathcal{N}_\xi}(\mathcal{Y}^{\ell}_{\nu\to\xi,\tau} - \mathcal{Y}^{\ell}_{\xi\to\nu,\tau}) + \mathcal{W}^{\ell}_{\xi,\tau}, \tag{13}$$

where the term $\mathcal{W}^{\ell}_{\xi,\tau}$ controls the local inflow and outflow of pedestrians for the network if ξ is a boundary cell.

3 Empirical fundamental diagrams and model implementation

3.1 Statistical Analysis

Efforts were made to base the class-specific fundamental diagrams in the implementation of the model on empirical results. The dataset used is part of the PedFlux project in collaboration with the CFF and consists in space and time observations of pedestrians in the western pedestrian underpass of the Lausanne train station during peak morning hours. The dataset is particularly useful in the context of this project as the camera system is designed to track individuals through the network [1]. Thus, in order to identify potential sub-populations with differing preferred walking speeds, the instantaneous speed of each pedestrian at each time step is calculated as the displacement in position during that time step over the length of the time interval. We also considered a smoother calculation of speed by the displacement over several time intervals centered at the interval in consideration. Several methods for determining the preferred walking speed of each pedestrian were then considered. Figure 1 shows the distribution of proposed preferred pedestrian speeds using the mean, median, mode and maximum speed of each pedestrian's set of instantaneous

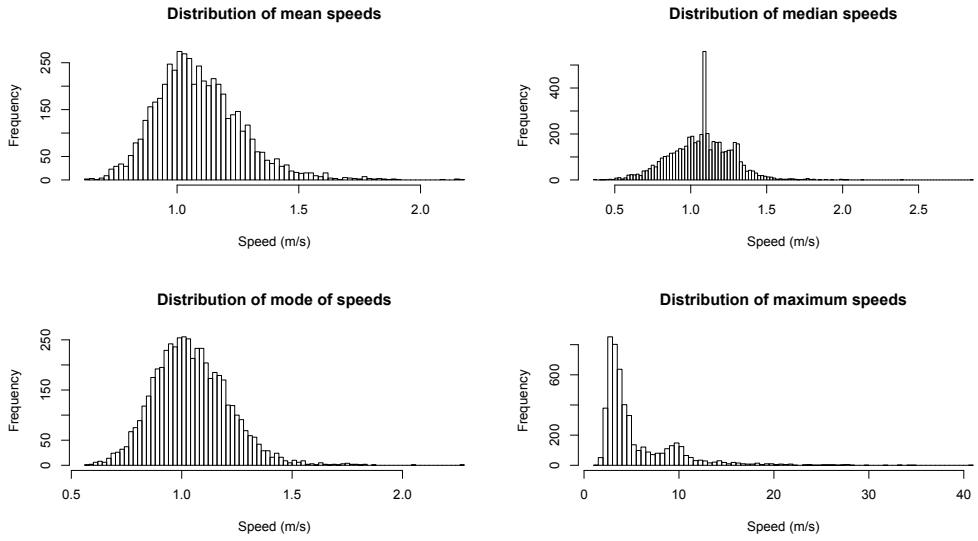

Figure 1: Distribution of preferred pedestrian walking speeds using the mean, median, mode and maximum of each pedestrian's instantaneous speeds.

speeds. The mode of a pedestrian's instantaneous speeds is calculated through a kernel density estimate using a bandwidth of 1.

We see that the distribution of preferred speeds using the mean and mode of pedestrian speeds are quite similar and reasonable with a peak slightly above 1.0 m/s. The distribution of preferred speeds using the median approach has an unrealistically sharp peak at around 1.1 m/s, which is most likely an artifact of the data collection process. The distribution of preferred speeds using the maximum of each pedestrian's instantaneous speeds also yields unrealistic results with significant mass at around 10 m/s, which is certainly a result of noise in the system.

In order to identify sub-populations from among the total population of pedestrians we employ a mixture model approach where we presume that the sub-populations have preferred walking speeds that are distributed normally in accordance with Weidmann's work [16]. An expectation-maximization algorithm is then used to identify the parameters of the sub-populations where the number of sub-populations is an explicit variable of the algorithm. Figure 2 shows the inferred distribution of preferred speeds of the sub-populations over the histogram of preferred speeds in the total population where two and three sub-populations are considered and the preferred speeds are calculated using the mode approach. We see in each case that one of the sub-populations is always small in amplitude and with a very large variance comparatively. This is most likely to accommodate the fit to noisy data points with unrealistically large preferred speeds in the distribution's upper tail. In both cases, this sub-population is ignored. Having inferred the distribution of preferred speed for each sub-population, we can calculate with what probability each individual pedestrian belongs to each sub-population. In this way, we can sort all the pedestrians into one sub-population or another depending on which one the pedestrian most likely belongs to.

Having sorted pedestrians into sub-populations, we can begin to identify the class-specific fundamental diagram of the sub-population. Density is estimated using the adapted Voronoi

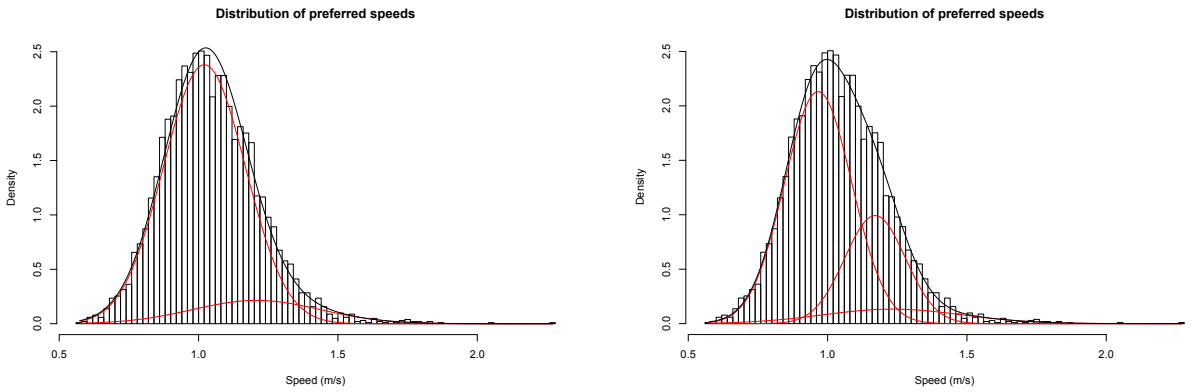

(a) (b)

Figure 2: Fit of the estimated preferred speed distribution of sub-populations to the empirically observed distribution of preferred speed in the total population. The red plots are the scaled and estimated density functions of the sub-population distributions and the black plots are the sum of the two. (a) two sub-populations. (b) three sub-populations

scheme developed by Nikolić [11]. In this analysis, we adopt Nikolić's approach and presume that within a sub-population and at a fixed pedestrian density k, space-mean speed is distributed as a Kumaraswamy distribution with parameters $\alpha(k)$ and $\beta(k)$, lower bound 0 and upper bound $u(k)$. The Kumaraswamy distribution is chosen as it has lower and upper bounds as a physically realistic distribution for space-mean speed would have. In addition, it can be asymmetric depending on the values of α and β and so we do not place strict assumptions on the distributional form of space-mean speed by this choice. The functional form of $\alpha(k)$, $\beta(k)$ and $u(k)$ are not specified but depend on a further set of underlying parameters denoted $\mathcal{K}$. Estimates for the parameters in $\mathcal{K}$ are obtained by maximizing the log-likelihood of the fit of the Kumaraswamy distribution to the dataset of instantaneous speeds as a function of local pedestrian density. In turn, class-specific and deterministic fundamental diagrams are calculated as the mode or mean of the underlying Kumaraswamy distribution at each density level.

This portion of the project yielded the least successful results in the scope of the overall work. There was great difficulty in selecting functional forms for the parameters $\alpha(k)$, $\beta(k)$ and $u(k)$ as well as initial guesses for the underlying parameters, $\mathcal{K}$, that would lead to a converged solution in a reasonable amount of time. In addition, all successfully converged solutions lead to estimates of the fundamental diagrams that predicted non-zero space-mean speeds or even increasing space-mean speeds as pedestrian density increases to infinity. In reality, one would expect the space-mean speed of all sub-populations to decrease to zero at some critical jam density. A key potential source of problems in this analysis is the presence of systematic noise in the dataset as seen in Figure 3, where the scatter plot of pedestrian speed against local density is presented at very high resolution.

We see that a significant portion of the observations occur along lines of fixed pedestrian speed, the most significant of which occurs at approximately 1.3 m/s. These lines extend out to the highest pedestrian densities observed. As a consequence, it is unsurprising that

Figure 3: High resolution scatter plot of observed instantaneous speeds as a function of local pedestrian density.

any attempt to fit a probability distribution with regression forms for the parameters to this dispersion will predict a fundamental diagram with constant or increasing space-mean speed as a function of local density. The high density of observations with fixed speed over density are most likely artifacts of algorithms in the data collection process that attempt to interpolate the positions of pedestrians in blind spots of the camera system.

Having failed to derive our own empirically inferred class-specific fundamental diagrams, we turn to empirical results from literature for the functional form of the space-mean speed over pedestrian density relation.

3.2 Model implementation

For the specific implementation of the proposed model, we choose to adopt the Kladek formula for the formulation of the speed-density relation as proposed by Weidmann [16]. Thus,

$$v^d(k) = v_f^d\Big(1 - \exp\big[-\gamma^d\Big(\frac{1}{k} - \frac{1}{k_c}\Big)\big]\Big), \;\; \forall d \in D, \tag{14}$$

where k_c is the jam density of pedestrians and is equal to N_ξ/A_ξ for a given cell ξ. We can easily see that an increase in the value of the parameter γ^d will lead to a more rapid decrease in space-mean speed as k increases and thus higher values of γ^d correspond to pedestrian classes with a higher sensitivity to congestion. From Equation (6), we find that the corresponding form for the cumulative hydrodynamic flow of class d pedestrians from

cell ξ to ν at time step τ is

$$Q^d_{\xi\to\nu,\tau} = M^d_{\xi,\tau}\Big(1 - \exp\big[-A_\xi \times \gamma^d\Big(\frac{1}{M_{\xi,\tau}} - \frac{1}{N_\xi}\Big)\big]\Big). \tag{15}$$

The route-choice formulation relies on the assignment of route- and class-specific cell potentials to each cell of the network. Each cell is assigned a route-specific, static floor field $\mathcal{F}^\rho_\xi$ that represents the minimum number of cells that must be traversed from ξ to reach the destination cell of route ρ. $\mathcal{F}^\rho_\xi$ can be easily calculated by using, for example, Dijkstra's algorithm. In addition, each cell is assigned a traffic-dependant and class-specific dynamic floor field $\mathcal{H}^d_{\xi,\tau}$ that is set equal to the fraction of the class d free-flow speed that the associated pedestrians can attain in the cell during time step τ. That is, $\mathcal{H}^d_{\xi,\tau} = v^d(M_{\xi,\tau}/A_\xi)/v^d_f$. The cell potentials are in turn defined by a linear combination of the two cell fields,

$$\mathcal{P}^{d,\rho}_{\xi,\tau} = \alpha\mathcal{F}^\rho_\xi - \beta\mathcal{H}^d_{\xi,\tau}, \tag{16}$$

where the parameters α and β are positive real numbers. In the implementation, α and β can be class-specific parameters but are taken here as class generic for the purposes of our investigations. The group-specific turning proportion from cell ξ to ν is then defined for an arbitrary group $\ell \in \mathcal{L}$ as

$$\delta^{\rho_\ell,d_\ell}_{\xi\to\nu} = \frac{\exp\{-\mathcal{P}^{d_\ell,\rho_\ell}_{\nu,\tau}\}}{\sum_{\nu'\in\Theta^{\rho_\ell}_\xi}\exp\{-\mathcal{P}^{d_\ell,\rho_\ell}_{\nu',\tau}\}}, \tag{17}$$

where $\Theta^{\rho_\ell}_\xi$ is the set of neighbors of ξ that are a part of route ρ_ℓ. We see from Equations (16) and (17) that a comparatively high value of α with respect to β will lead to en-route path choice that will follow the shortest path to the destination as closely as possible. Conversely, a relatively high value for β will favor routes that avoid cell congestion as much as possible. The priority structures are determined by the assignment of dynamic, class-specific values to each cell in the network at the start of each time step. In our implementation, these values take the form

$$\mathcal{G}^d_{\xi,\tau} = \lambda v^d(M_{\xi,\tau}/A_\xi) + \mu M^d_{\xi,\tau}, \tag{18}$$

where λ and μ are real parameters of the model. Once again the parameters λ and μ could in principle be class-specific, cell-specific or time varying as well but are taken as entirely generic in the implementation. The ordering within the priority structure for each class is determined by the relative values of $\mathcal{G}^d_{\xi,\tau}$, with the highest priority going to the class with the highest value and downward from there in descending order of the $\mathcal{G}^d_{\xi,\tau}$ values. We see that a high value of λ compared to μ will systematically give priority to those classes with the higher space-mean speeds in the cell. Conversely a comparatively high value of μ will give priority within each cell to the classes with the highest local density at each time step. This system can also be extended to a stochastic model by having the $\mathcal{G}^d_{\xi,\tau}$ values be the expected values of random variables whose shared variance is also given as a parameter of the model. Our implementation includes this option where the random variables are normally distributed. For the limited purposes of our investigations we will consider only three alternative priority

	Parameter	Value
Generic Parameters	ΔL	1.0 m
	A_ξ	1.0 m^2
	k_c	5.4 peds/m^2
	α	2.0
	β	0.0
d_1 Parameters	$v_f^{d_1}$	1.5 m/s
	γ^{d_1}	1.9 $1/m^2$
d_2 Parameters	$v_f^{d_2}$	1.0 m/s
	γ^{d_2}	1.9 $1/m^2$

Table 1: Parameter values for test case 1

structure schemes. The first scheme, Priority A, assigns priority as a function of free-flow speed where the faster classes get priority. This is achieved by the choice $(\lambda, \mu) = (1, 0)$. The second scheme, Priority B, gives priority to the classes with smallest free-flow speeds by setting $(\lambda, \mu) = (-1, 0)$. Priorities A and B are both static and spatially homogeneous priority structures as they remain the same throughout the cell network at every time step of the simulation. The last priority scheme, Priority C, assigns priority to the classes in a cell with the highest pedestrian density. Priority C is a dynamic and cell varying priority scheme and is achieved by choosing $(\lambda, \mu) = (0, 1)$.

4 Numerical simulations and analysis

The specific physical layout of the cell network that will be utilized for our investigations is that of either a 30 or 60 meter long by 1 meter wide corridor that is composed of unit cells end to end. Pedestrian groups will enter and leave the network only at the boundary cells located at either end of the corridor. We are specifically interested in modeling pedestrian heterogeneity with respect to varying free-flow speeds. Thus, the sensitivity to congestion parameters for all classes are set equal to 1.9 1/meters^2 and the area of each cell is held fixed at $\Delta L^2 = 1$ meters^2. In addition, the class-generic jam density parameter is taken to equal 5.4 pedestrians/meter^2. These values are chosen to be in accord with Weidmann's empirical findings [16] and so as to give these simulations a grounding in reality.

4.1 Bi-class test cases

The first suite of tests involve the interactions between two classes of pedestrians with differing free-flow speeds. The set D is thus here equal to $\{d_1, d_2\}$. Table 1 is a summary of the parameter values chosen for this particular set of investigations. We see that the first class, d_1, is comparatively fast with a free-flow speed of 1.5 m/s while the second class, d_2, has a free-flow speed of 1.0 m/s. The route-choice parameters are chosen such that only the minimum distance to the target cell is considered. As we are considering the simple case of corridor motion, the inclusion of a sophisticated en-route path strategy, taking into account the relative pedestrian density of neighboring cells, would be superfluous.

4.1.1 Unidirectional flow

The first set of tests involve unidirectional flow along the 60 meter corridor. The slower class, d_2, leaves one end of the corridor at time step 0 and a pre-chosen amount of time later the faster class, d_1, leaves from the same end. The time delay for departure of the d_1 class is 16 time steps and is chosen such that a good picture of the waveforms of each class is visible before, during and after the phases that the d_1 pedestrian group overtakes the d_2 pedestrians.

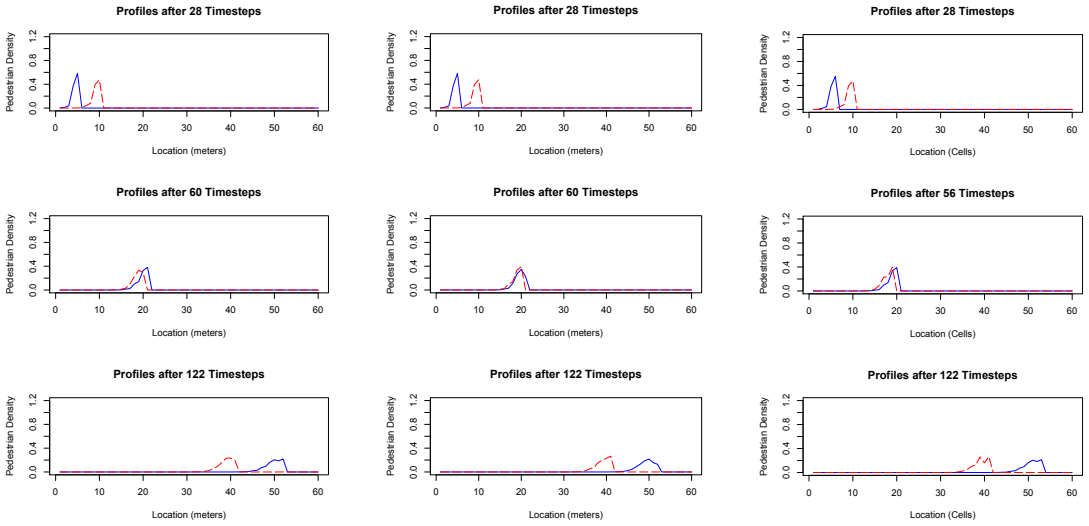

(a) (b) (c)

Figure 4: Low congestion, unidirectional flow tests. (a) Priority A test. (b) Priority B test. (c) Priority C test. In all tests, the blue solid line is the waveform of class d_1 pedestrians and the dashed red line is that of d_2 pedestrians.

Figure 1 gives a picture of these waveforms at 3 time slices for the 3 different priority schemes at a relatively low level of congestion. The demand load is equal to 1.0 pedestrians per class thus the first cell is at approximately 20% cell capacity at the departure time of each class. We see that similar behavior is displayed across all three priority schemes. By time step 122, the waveforms in all three priority schemes are located in the same location along the corridor and have very similar relative shapes. The fact that the differing priority structures have a minimal impact on the simulation is an expected result in low congestion cases.

Figure 5 shows the same series of tests for the case of higher congestion. The initial demand load for both classes is now 3.0 pedestrians and thus is over 50% of cell capacity in both cases. We see that Priorities A and C have largely the same results with only very slight differences in waveform shape by time step 134. In contrast, the behavior of the faster class is quite different for the case of Priority B. As the waveform of the d_1 pedestrians approaches the slower group from behind, the majority of the d_1 pedestrian mass becomes concentrated at the back tail of the d_2 waveform because d_2 has systematic priority. As the two waveforms advance, the front tail of d_1 gradually seeps forward, stretching out the shape of the class's

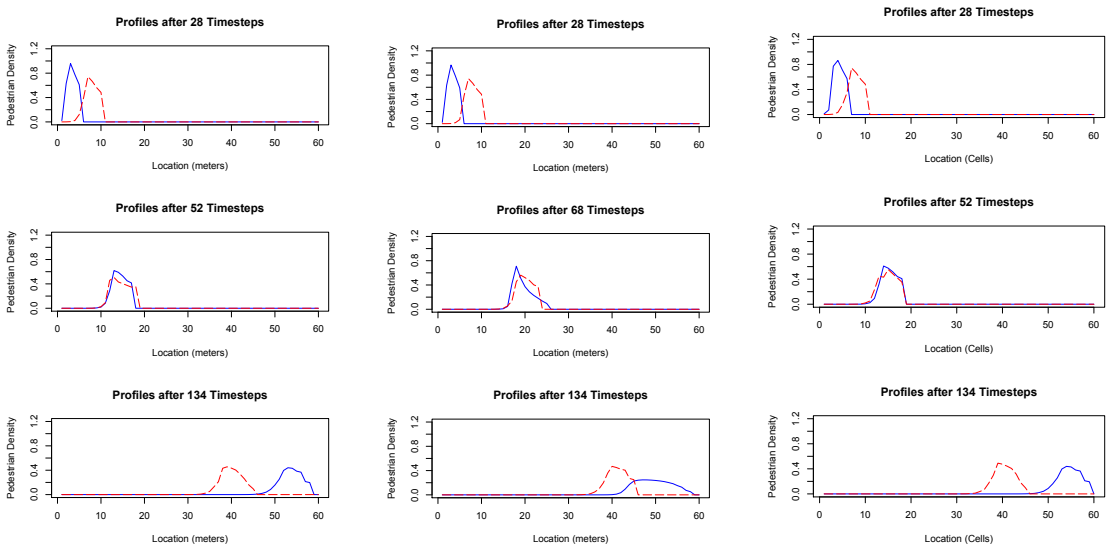

(a) (b) (c)

Figure 5: High congestion, unidirectional flow tests. (a) Priority A test. (b) Priority B test. (c) Priority C test. In all tests, the blue solid line is the waveform of class d_1 pedestrians and the dashed red line is that of d_2 pedestrians.

waveform until the d_1 pedestrians have almost entirely overtaken the other class by time step 134. Not only is there a large difference in the shape of the d_1 waveform by this time step, but the average location of the waveform also appears several cells behind those seen in the other two priority schemes.

4.1.2 Bidirectional flow

In these simulations, a group of pedestrians of the slower class d_2 leaves the right side of the 60 meter corridor at time step 0, followed by a pedestrian group of class d_1 leaving the left side 16 time steps later. The delay in departure time for the faster class is chosen so as to ensure that the pedestrian groups cross at approximately the mid-point of the corridor. The demand load for each pedestrian group is 8.0 pedestrians and is thus at nearly 150 % cell capacity for both classes. We see in Figure 6 that even at this high pedestrian demand density there is seemingly zero difference in the waveforms of the two classes at the respective time slices across all priority schemes. This result is to be expected as the flow constraints of outflow and inflow capacities for each class along the links of a cell can only be affected by pedestrian groups flowing in the same direction. As such, since the two pedestrian groups are traveling in opposite directions with little backward motion there is little to no competition for flow along the directed links of any cell and thus the priority schemes make virtually no difference to the outcome of the simulation.

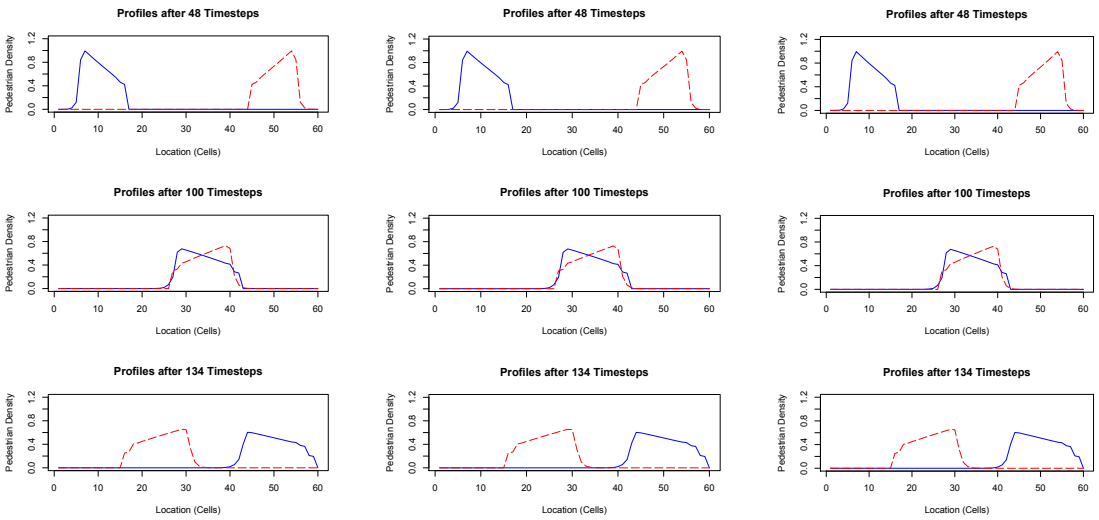

(a) (b) (c)

Figure 6: High congestion, bidirectional flow tests. (a) Priority A test. (b) Priority B test. (c) Priority C test. In all tests, the blue solid line is the waveform of class d_1 pedestrians and the dashed red line is that of d_2 pedestrians.

4.2 Modeling population heterogeneity

One of the most significant problems with the homogeneous model is related to the particular shape of pedestrian groups in unidirectional motion. A weighted histogram plot of arrival times for a pulse of homogeneous pedestrians in the 30 meter corridor as shown in Figure 7 illustrates this point. We see that the bulk of the pedestrian density occurs at the earliest observed arrival time and decreases monotonically thereafter as arrival time increases. According to Weidmann's research [16], the preferred free-flow speeds within a population of pedestrians is normally distributed with a mean of 1.34 m/s and a standard deviation of 0.34 m/s. While this distribution is only approximative, particularly given that a normal distribution has infinite support, it is still useful in guiding intuition. If the distribution of free-flow speeds is indeed shaped thusly, one would expect the distribution of arrival times in reality to be approximately unimodal, continuous and asymmetric with a heavy upper tail. By modeling free-flow speed heterogeneity with increasingly more classes in the pedestrian population, we can investigate how well our system approximates this expected limiting distribution in contrast to the homogeneous model. In the interest of brevity, these simulations are all fixed at a low degree of congestion of 1.0 pedestrians across all classes and utilize only Priority C as a priority scheme. We use Weidmann's empirical relation and scale the demand load of each class to the density value of the above gaussian at the free-flow speed of the considered class. We conduct three simulations, using 3, 6 and 10 classes respectively where the value of each class's free-flow speed and pedestrian demand load are given in Table 2. These tests use the 30 meter corridor and, contrary to the previous unidirectional simulations, all pedestrian groups leave the leftmost end of the corridor at the same time step 0.

Figure 8 shows the weighted histogram plots of arrival times for the three simulations

	Parameter	Value
2 class simulation	$v_f^{d_1}$	1.2 m/s
	demand:	0.4827059
	$v_f^{d_2}$	1.4 m/s
	demand:	0.5172941
6 class simulation	$v_f^{d_1}$	0.8 m/s
	demand:	0.07190368
	$v_f^{d_2}$	1.0 m/s
	demand:	0.15394156
	$v_f^{d_3}$	1.2 m/s
	demand:	0.23317704
	$v_f^{d_4}$	1.4 m/s
	demand:	0.24988533
	$v_f^{d_5}$	1.6 m/s
	demand:	0.18946144
	$v_f^{d_6}$	1.8 m/s
	demand:	0.10163095
10 class simulation	$v_f^{d_1}$	0.4 m/s
	demand:	0.005152284
	$v_f^{d_2}$	0.6 m/s
	demand:	0.022037098
	$v_f^{d_3}$	0.8 m/s
	demand:	0.066685914
	$v_f^{d_4}$	1.0 m/s
	demand:	0.142770640
	$v_f^{d_5}$	1.2 m/s
	demand:	0.216256313
	$v_f^{d_6}$	1.4 m/s
	demand:	0.231752152
	$v_f^{d_7}$	1.6 m/s
	demand:	0.175712982
	$v_f^{d_8}$	1.8 m/s
	demand:	0.094256002
	$v_f^{d_9}$	2.0 m/s
	demand:	0.035771675
	$v_f^{d_10}$	2.2 m/s
	demand:	0.009604939

Table 2: Parameter values for the multi-class simulations

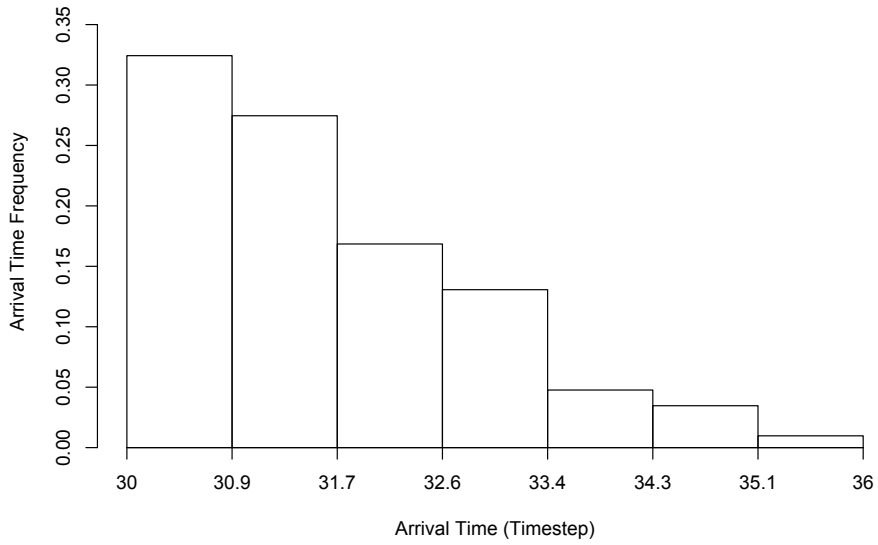

Figure 7: Weighted histogram of arrival times for a homogeneous population of pedestrians.

where the number of bins in the histograms is held fixed at 30 across all tests. This gives each histogram approximately the same scale of temporal resolution. We see that across all three tests, the distribution of arrival times is more complex than that seen in the homogeneous population of Figure 7. In particular, we note that the approximate structure of the expected limiting distribution becomes more apparent as the number of classes is increased. The third simulation best conveys the emergence of a unimodal distribution with a short lower tail and heavy upper tail. As an aside, we get an indication for the increased numerical burden of increasing the number of classes by the scale of the horizontal axis across all three simulations.

Figure 9 shows the spatial distribution of the pedestrians across 4 time slices in the 60 m long corridor where 6 classes are used to model population heterogeneity. The model parameters are identical to those used in the previous 6-class simulation as shown in Table 2 with the exception that the demand load of each class is now three times greater. Once again, Priority C is used as the priority scheme. We see that the distance between the classes's average location increases as time progresses and that this distance appears to increase more so for the slower classes. We also see that the congestion in the network disproportionately affects the faster pedestrian classes. This makes sense as the fastest classes will tend to give priority to the classes with free-flow speeds closest to the average of 1.34 m/s. As all the pedestrian groups commence in the same source cell, the faster classes must seep through the slower classes with higher priority in order to reach the front of the pack. This stretches out the waveform of the fast classes in the same way as seen in Figure 5 for the Priority B case. Indeed, this process is visible in stages across the time slices in particular for pedestrian classes d_5 and d_6.

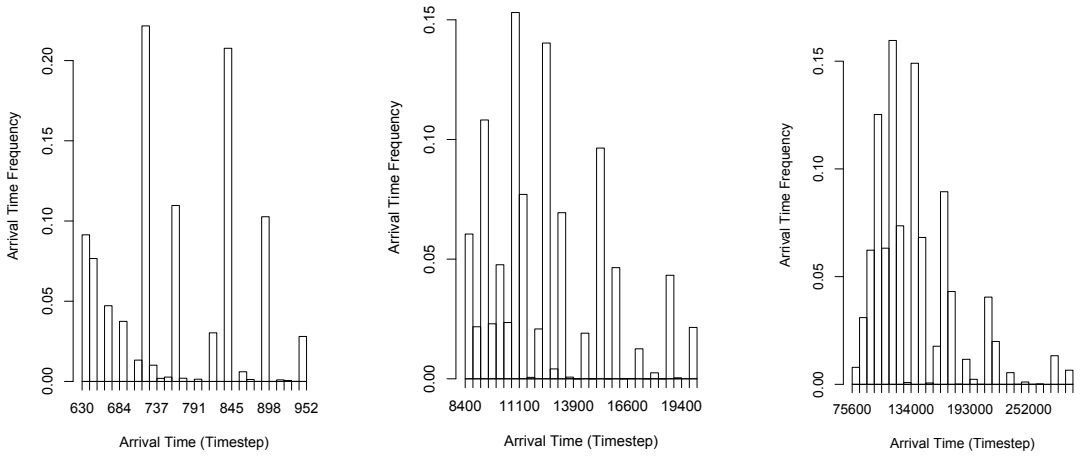

(a) (b) (c)

Figure 8: Weighted histogram plots of arrival times for the multi-class simulations. (a) 3 classes. (b) 6 classes. (c) 10 classes.

5 Conclusions

5.1 Summary

This work consisted of the development, implementation and analysis of a cell transmission model for simulating multidirectional pedestrian flows in walking areas. The model is an extension of the previously developed PedCTM, which presumes that pedestrian populations are homogeneous and have a common fundamental diagram. Pedestrian heterogeneity is accounted for in the developed model through a multi-class framework in which each class of pedestrians is characterized by its own fundamental diagram. This approach uses the implementation of an update cycle with differing time interval discretizations across pedestrian classes in order to minimize the numerical dispersion of pedestrian flows. The principle proposal of this model is the assumption that at each link of the cell network and at each time step, pedestrian classes are sorted into priority queues and flow one after another in an orderly fashion. The actual ordering of the priority schemes need not be static or homogeneous across the cell network. Further, the numerical implementation of the model even includes the option of stochastic priority queues. The numerical implementation made use of Weidmann's empirical results for the form of the fundamental diagrams as well as for the values of key parameters. A set of test cases intended primarily as a proof of concept was presented.

5.2 Potential issues with the model

The principle theoretical issue with the developed model relates to the priority structure as there is no justification for the scheme in the kinematic wave model. A central goal of any

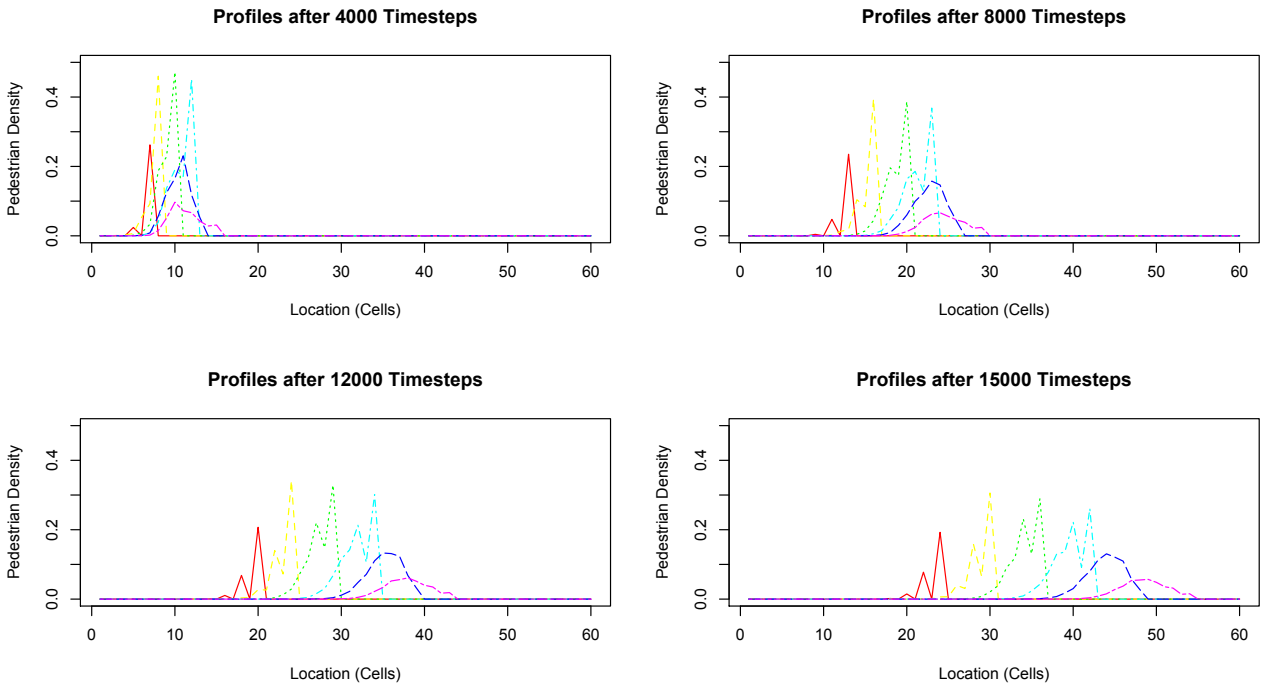

Figure 9: Spatial distribution of pedestrians across 4 time slices with 6 pedestrian classes. red: d_1, yellow: d_2, green: d_3, light blue: d_4, dark blue: d_5, pink: d_6.

numerical discretization scheme is to recover the results of the continuum model in the limit as the discretization density goes to infinity. In our model however, the flow of pedestrians is affected by a priority framework that acts along the edges of the cell network. If we then split all cells into four cells by setting $\Delta L = 1/4$, we have new interfaces for the sorting of flows at the center of the cell where none existed before. In the limit, the flow of pedestrians will be an artifact of the priority scheme entirely and not of underlying pedestrian dynamics.

In addition, there is a potential issue with the cell-specific flow constraint in Equations (11) and (12). The step renormalizes all the flows into a cell if the flow would otherwise exceed the capacity of the cell. This is problematic as the flow into one side of the cell can be affected by the flow into other sides of the cell which is non-local to the flow considered. This can lead to numerical instability and potentially the formation of shockwaves were none would otherwise occur.

A systematic analysis of the model with respect to the potential formation of shockwaves and the effect of the priority scheme as the cell density increases would be of interest to explore the ramification of these issues.

5.3 Future areas of research

The numerical simulations and results presented in this work do not serve by any means as an exhaustive analysis of the capacities and implications of the model. In this vein, further analysis that explores the behavior of pedestrian classes with differing sensitivities to congestion, en-route path strategies and asymmetric densities is possible for example. In addition,

a complete analysis of the effect of priority schemes, both dynamic and stochastic, is within the capacities of the numerical implementation. From a more empirical perspective, it would be of interest to base the functional form and parameters of the class-specific fundamental diagrams off statistical inference from real-world data. A mixture model approach to inferring the presence of pedestrian sub-populations is one potential course. Alterations to the code that would reflect such findings would be minimal. Further amendments to the code, in the interest of computational efficiency and speed, are also needed. Another potential avenue for future work would be to generalize the model to account for spatial as well as population heterogeneity. The inclusion of the update cycle in particular makes the model easily extendable in this direction. We would also be interested in further model validation tests that investigate to what extent and in what situations the heterogenous model is preferable to the less computationally costly homogeneous model. Ultimately, however, further explorations into extending PedCTM to population heterogeneity using a multi-class approach without reliance on the proposed priority scheme are desirable.

References

[1] Alahi, A., Jacques, L., Boursier, Y. and Vandergheynst, P. (2011). Sparsity driven people localization with a heterogeneous network of cameras, *Journal of Mathematical Imaging and Vision,* **41**(1-2) 3958.

[2] Al-Gadhi, S. A. and Mahmassani, H. S. (1991). Simulation of crowd behavior and movement: fundamental relations and application, *Transportation Research Record* **1320**(1320): 260268.

[3] Asano, M., Sumalee, A., Kuwahara, M. and Tanaka, S. (2007). Dynamic cell transmission-based pedestrian model with multidirectional flows and strategic route choices, *Transportation Research Record: Journal of the Transportation Research Board* **2039**(1): 4249.

[4] Dafermos, S. C. (1972). The traffic assignment problem for multiclass-user transportation networks, *Transportation Science* **6**(1): 7387.

[5] Daganzo, C. (1994). The cell transmission model: A dynamic representation of highway traffic consistent with the hydrodynamic theory, *Transportation Research Part B: Methodological* **28**(4): 269287.

[6] Daganzo, C. (1995). The cell transmission model, Part II: Network traffic, *Transportation Research Part B: Methodological* **29**(2): 7993.

[7] Guo, R., Huang, H. and Wong, S. (2011). Collection, spillback, and dissipation in pedestrian evacuation: A network-based method, *Transportation Research Part B: Methodological* **45**(3): 490506.

[8] Hänseler, F., Bierlaire M., Farooq, B. and Mühlematter T. (2013). An aggregate model for transient and multidirectional pedestrian flows in public walking areas, *Technical Report,* **TRANSP-OR 131219,** Transport and Mobility Laboratory, Ecole Polytechnique Fédérale de Lausanne.

[9] Hughes, R. L. (2002). A continuum theory for the flow of pedestrians. *Transportation Research Part B: Methodological*, **36**(6), 507-535.

[10] Lighthill M. J., Whitham G. B. (1955). On Kinematic waves. 2. A theory of traffic flow on long crowded roads. *Proc R Soc London Ser A* 229:317345.

[11] Nikolić, M., Bierlaire, M., and Farooq, B. (2014). Probabilistic speed-density relationship for pedestrians based on data driven space and time representation. *Proceedings of the Swiss Transportation Research Conference (STRC)* 14 - 16 May, 2014.

[12] Richards, P. I. (1956). Shock waves on the highway. *Operations research,* **4**(1), 42-51.

[13] Seyfried, A., Steffen, B., Klingsch, W. and Boltes, M. (2005). The fundamental diagram of pedestrian movement revisited, *Journal of Statistical Mechanics: Theory and Experiment* **2005**(10): P10002.

[14] Steffen, B. and Seyfried, A. (2010). Methods for measuring pedestrian density, flow, speed and direction with minimal scatter, *Physica A: Statistical mechanics and its applications,* **389**(9) 19021910.

[15] Van Wageningen-Kessels, F. (2013). Multi-class continuum traffic flow models: analysis and simulation methods. *In PhD thesis, Delft University of Technology.*

[16] Weidmann, U. (1993). *Transporttechnik der Fussgänger, Institute for Transport Planning and Systems*, ETH Zürich.